ChemComm

COMMUNICATION

View Article Online
View Journal | View Issue

Published on 19 May 2014. Downloaded by Washington University in St. Louis on 04/10/2014 11:10:01.

Cite this: *Chem. Commun.*, 2014, **50**, 8723

Received 8th April 2014,
Accepted 19th May 2014

DOI: 10.1039/c4cc02564d

www.rsc.org/chemcomm

Novel highly emissive H-aggregates with aggregate fluorescence change in a phenylbenzoxazole-based system†

Lianke Wang,[a] Yanfang Shen,[a] Mingdi Yang,[ab] Xiuzhen Zhang,[c] Weinan Xu,[a] Qiuju Zhu,[a] Jieying Wu,[a] Yupeng Tian[a] and Hongping Zhou*[a]

Fibrous nanoaggregates of a new benzoxazole-based derivative have been reported. This derivative exhibits not only H-aggregates but also strong yellow fluorescence, which is different from the traditional understanding of H-aggregates.

Designing novel chromophores with excellent optical properties in the condensed state has been a popular research area because of their potential applications in organic light emitting diodes (OLEDs),[1] fluorescent sensors,[2] *etc.* The restriction of intramolecular rotation (RIR) or planarization and J-aggregation reported by Tang[3] and Park[4] favor enhanced emission. The frequently reported aggregation-caused quenching fluorescence (ACQ)[5] in H-aggregates has greatly limited their potential applications. At present, various excellent chromophores with aggregation-induced emission[3] or enhanced emission[4] (AIE/AIEE) properties have been developed by many research groups, such as tetraphenylethene,[6] cyanostilbene[7] and 9,10-distyrylanthracene derivatives,[8] which all avoid H-aggregation.

Considering the interesting fluorescence properties of benzoxazole, we utilized benzoxazole as building blocks and changed the terminal substituents to build new phenylbenzoxazole-based chromophores. The structures of the target molecules are shown in Scheme 1 (see also ESI† Scheme S1). In this communication, we reported the highly emissive H-aggregate **2b** and the unique AIEE phenomenon with large red shifts and remarkable color change. Thermogravimetric analysis (TGA) and differential scanning calorimetry (DSC) results indicate that all 3 prepared compounds possess high melting points with T_m at 139.9, 235.8 and 201.9 °C (Table 1), respectively, and high thermal stability with T_d at 294, 273 and 294 °C (Table 1), respectively.

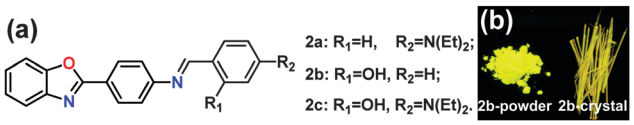

Scheme 1 (a) The molecular structures of **2a**, **2b** and **2c**, (b) photographs of powder and crystals of **2b** under UV light.

We initially investigated the absorption and fluorescence spectra of **2a–2c** (10 μM) in various polarity solvents (Table S1 and Fig. S1, ESI†). The absorption and fluorescence spectra of **2a–2c** demonstrate quite similar maxima in the different solvents, indicating a slight solvent dependence. The target molecules show strong absorption bands at 388, 327 and 414 nm, respectively, and emission maxima (λ_{em}) at 499, 389 and 495 nm, respectively. The weak absorption peaks at 300–320 nm are mainly attributed to π–π* electronic transitions derived from the benzoxazolyl-benzene unit.[9] The molar extinction coefficient values also are in agreement with π–π* transitions.[10] Theoretical calculations are a reliable method for qualitative indication of the absorption properties.[11] We calculated the frontier molecular orbitals based on the molecular

Table 1 Optical properties of the target molecules

		λ_{em}/nm					
Compd	λ_{abs}/nm	Pure	Mixed	Powder	Crystal	T_m (°C)	T_d (°C)
2a	388	499	518	552	593	139.9	294
2b	327	389	542	581	588	235.8	273
2c	414	495	564	564	564	201.9	294

λ_{abs} = the maxima absorption peak, λ_{em} = the maxima emission peak, in dilute ethanol solution (10^{-5} mol L^{-1}), pure = pure ethanol solution, mixed = a mixed water–ethanol solution with f_w = 0.90, T_d = temperature for 5% weight loss, T_m = melting temperature recorded using a differential scanning calorimeter.

[a] *College of Chemistry and Chemical Engineering, Key Laboratory of Functional Inorganic Materials Chemistry of Anhui Province, Anhui University, Hefei 230601, P. R. China. E-mail: youthmd98@163.com, zhpzhp@263.net; Fax: +86-551-63861279; Tel: +86-551-63861279*

[b] *Key Laboratory of Opto-Electronic Information Acquisition and Manipulation of Ministry of Education, Anhui University, Hefei 230601, P. R. China*

[c] *Center of Modern Experimental Technology, Anhui University, Hefei 230039, P. R. China. E-mail: ahzhangxz@ahu.edu.cn*

† Electronic supplementary information (ESI) available: Synthesis, characterization, spectra, SEM images and theoretical calculations. CCDC 994632–994634. For ESI and crystallographic data in CIF or other electronic format see DOI: 10.1039/c4cc02564d

Published on 19 May 2014. Downloaded by Washington University in St. Louis on 04/10/2014 11:10:01.

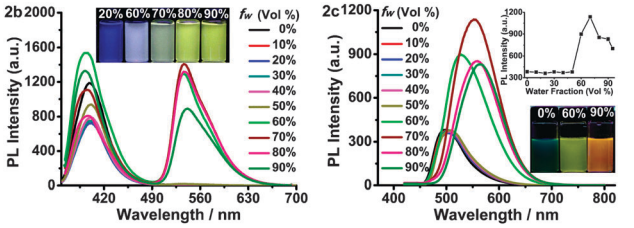

Fig. 1 The fluorescence spectra of **2b** and **2c** in water–ethanol mixtures with different water fractions (f_w). The inset depicts the changes of PL peak intensity with different f_w. Photos of **2b** and **2c** in water–ethanol mixtures with different f_w, taken under UV light. Concentration: 50 μM.

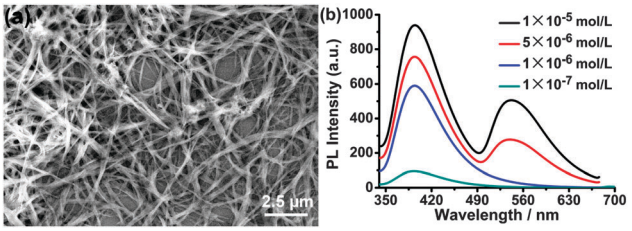

Fig. 2 (a) SEM image of the nanoaggregates of **2b** prepared in an ethanol/water (2 : 8) mixture at a concentration of 50 μM. (b) The PL spectrum of **2b** in different concentrations with f_w = 80%.

conformations in the crystal structures. Further details are given in the ESI† and the results are in good agreement with the experimental absorption spectra. All data indicate that the introduction of diethylamino groups can change the π-conjugation degree of benzoxazolyl compounds.

2a–2c exhibit weak green, blue and cyan emissions in diluted ethanol solution under UV light (inset in Fig. S2, ESI† and Fig. 1), respectively. Firstly, the fluorescence intensity of **2a** is almost linearly increasing step-by-step with the increasing of water fraction, accompanied with a red-shift in the λ_{em} values. The light emission reaches its maximum value when f_w = 70%, which is 6.4-fold higher than that in pure ethanol solution. **2b** exhibits different fluorescent behavior in ethanol–water solutions with different f_w values. Upon addition of water, the emission intensity and wavelength show a slight decrease and a red shift, respectively. When $f_w \geq 60\%$ (Fig. 1), the yellow emission band centred at 542 nm rapidly turns on. The inset photos (Fig. 1) taken under UV light show the color change and we can clearly see that the blue solution vividly changes to yellow. In addition, **2c** also exhibits emission changes from cyan to orange with a red-shift of 70 nm after addition of the different amounts of water. The fluorescence intensity remain unchanged until f_w is increased to 60%, the solutions emit bright yellow light with λ_{em} at 528 nm. The emission intensity reaches its maximum value at f_w = 70% and the λ_{em} red-shifts to 564 nm when f_w = 90%. Such ratiometric fluorescence changes with large red-shifts of 150 and 70 nm for **2b** and **2c** in benzoxazole-based compounds have so far never been reported, not to mention the impressive color changes. These unique AIEE behaviors are very significant in the field of fluorescent probes. The absorption spectra of **2a** and **2c** show a slight bathochromic shift and a level-off tail in the long-wavelength regions. The tail is caused by the Mie scattering effect,[6] which suggests the formation of nanoaggregates. The absorption spectrum of **2b** exhibits a slight blue-shift and a few new absorption peaks arise between 370 and 420 nm when $f_w \geq 60\%$, which indicate the formation of new species.

To gain further insight into the unique morphology of the nanoaggregates of these benzoxazole-based compounds in the mixture system, the mixture solutions were subjected to scanning electron microscopy (SEM) observation. As can be seen from the photos shown in Fig. 2a and Fig. S3 (ESI†), the three benzoxazole-based compounds aggregate to form three different shapes in the mixture system. A large number of block nanoparticles of **2a** formed immediately in the mixture of ethanol–water with f_w = 80% (Fig. S3a, ESI†). It is noteworthy that **2b** molecules aggregate to form entangled three-dimensional networks consisting of interconnected fibrous nanoaggregates, which has so far never been reported in benzoxazole-based compounds (Fig. 2a).[12] **2c**, aggregates into rice-shaped nanoparticles in ethanol–water mixtures (Fig. S3c, ESI†). These morphologies must be responsible for the observed enhanced emission and the impressive color changes.

We also comparatively investigated their emissions in different states. Their normalized fluorescence spectra are shown in Fig. S4 (ESI†) and relative emission wavelength are shown in Table 1. All compounds exhibit the minimum emission wavelength in pure ethanol solution and the maximum emission wavelength in the crystalline state. **2a** and **2b** show the same trend: $\lambda_{em/Pure} < \lambda_{em/Mixed} < \lambda_{em/Powder} < \lambda_{em/Crystal}$, while **2c** displays $\lambda_{em/Pure} < \lambda_{em/Mixed} \approx \lambda_{em/Powder} \approx \lambda_{em/Crystal}$.

According to some other AIE/AIEE-active systems, the reasons for these unique fluorescent behaviors can be tentatively ascribed to the different molecular conformations and packing modes in the different states.[13] In pure ethanol solution, these compounds molecules are molecularly isolated without any interactions between the adjacent molecules, and the molecules have highly twisted conformations due to the intramolecular steric hindrance, which leads to the minimum λ_{em}. The molecules of **2a–2c** in the crystal state are arranged so regularly that the rotatable single bonds are locked due to the multiple physical intermolecular interactions (see the following crystal discussion). These increase the molecular planarity and strengthen the π-conjugated systems, which contribute to the maximum λ_{em}. The powder states have less regularity compared with that in the crystal states. In condensed solution, **2a** shows common features just like some other AIE/AIEE-active systems, while **2b** may form multimers in a mixture with high water content. The emission wavelength of **2c** in the mixed solution is close to that in the powder and the crystal states, suggesting that they originate from the same emitting species with similar molecular conformation and interactions.

To obtain a better understanding of the enhanced emission and impressive color change of **2a–2c**, we investigated their crystal structures. The single crystals were obtained by slow evaporation from ethanol, CH_2Cl_2–ethanol and CH_2Cl_2–CH_3CN solution, respectively and their crystallographic data are summarized in Table S2 (ESI†).

As shown in Fig. S5 (ESI†), due to the existence of intramolecular hydrogen bonds, they all have better planarity. The

 This journal is © The Royal Society of Chemistry 2014

Published on 19 May 2014. Downloaded by Washington University in St. Louis on 04/10/2014 11:10:01.

ORTEP diagram with atom numbering and high-dimensional structures of **2a** is shown in Fig. S6 (ESI†). The adjacent three molecules are cross-linked into a one-dimensional band in a face-to-edge way *via* multiple C–H···π interactions (d = 2.743, 2.823, 2.964 and 2.905 Å) and C–H···N hydrogen bonds (d = 2.780 and 2.747 Å). Furthermore, more molecules are interconnected by the above-mentioned intermolecular interactions to form two-dimensional layer structures. The molecular structure of **2b** in the crystal state is nearly coplanar (Fig. S7, ESI†). We can clearly see from Fig. S7c (ESI†) that the two molecules are initially cross stacked in edge-to-edge manner to form an L-shaped dimer through C–H···O hydrogen bonds between the hydroxystyryl hydrogen atoms and the hydroxy oxygen atom, with the distance measured at 2.716 and 2.680 Å, respectively. As shown in Fig. S7b (ESI†), two **2b** molecules are slip-stacking together in face-to-face type to form H-aggregates through π···π stacking interactions with the distance measured at 3.477 Å. The two dimers are then connected with each other in a middle-to-middle way to form a #-shaped tetramer through C–H···N (d = 2.564 Å) and C–H···O (d = 2.668 Å) hydrogen bonds between the hydrogen atoms of the benzoxazolyl and phenyl groups of one molecule and the nitrogen and oxygen atoms of the benzoxazolyl group of the adjacent molecule. The #-aggregates are further expanded to form a two-dimensional multimer crossing layer structure by the above-mentioned type of hydrogen bonds and π···π stacking interactions. The formation scheme of the two-dimensional expanded cross packing layer structure is shown in Fig. 3. For **2c**, its crystal structure is similar to that of **2a**. Fig. S9b (ESI†) shows all intermolecular interactions on one molecule, including C–H···π (d = 2.735, 2.844 and 2.852 Å), C–O···π (d = 3.010 Å) and C–H···N (d = 2.847 and 2.699 Å) interactions. **2c** molecules are linked into two-dimensional bands *via* the above intermolecular interactions (Fig. S9c, ESI†). Furthermore, these band structures are connected in a head-to-head way to form a three-dimensional W-shaped stacking structure by another type of hydrogen bond between the nitrogen atoms on the oxazolyl rings and the hydrogen atoms of phenyl rings, with the distance measured at 2.796 Å.

According to the crystal structures, the obvious enhanced emission and unique color change can be well explained by these existing multiple interactions. Under the synergetic effect of intra- and intermolecular interactions, intramolecular motions are locked and the molecular conformations are more rigid and planar. Thus, the physical restriction of intramolecular motions and aggregation-induced planarization induced by the molecular aggregation can be considered as the mechanisms of the enhanced emission phenomena of **2a** and **2c**. For **2b**, it is obvious that **2b** molecules have better planarity and aggregate to form multimers in face-to-face manner according to its crystal structure. In general, the formation of H-aggregates where molecules are aligned parallel to each other with strong intermolecular interactions is characterized by blue-shifted absorption bands, which tend to induce the non-radiative deactivation process.[14] The absorption bands and the crystal structures all prove that **2b** molecules aggregate to form H-aggregates. The formation of multimers shows an obvious concentration dependence. When the concentration of **2b** is lower than 1 μM in the ethanol/water (2 : 8) mixture, the yellow emission at 542 nm disappeared (Fig. 2b and Fig. S13, ESI†), which indicates the absence of the special emissive species that show yellow emission. Thus, we can speculate that the emission in the yellow region is attributed to the emission of H-aggregates, which is quite different from the traditional understanding of H-aggregates.

Generally, high radiative rates can efficiently enhance emission, while the active exciton migration is detrimental to emission.[15] Whether the emission quenches or strengthens is determined by the competition between the two opposite factors. Obviously, the positive effect is dominant in the emission process of **2b**. It is very likely that the specific slip-stacking and the dimer formed by multiple intermolecular hydrogen bonds play essential roles in its high emission, which effectively slow exciton motion, turn on radiative decay channel and avoid strong H-type coupling to some extent, thus H-aggregates of **2b** exhibit high emission.

Considering the color changes in solution and nanoaggregates, the application of **2b** nanoaggregates to detect highly volatile organic solvents was investigated on thin-layer chromatography plates (Fig. S12, ESI†). Under 365 nm UV light at room temperature, **2b** nanoaggregates show bright yellow fluorescence which turns blue in an atmosphere of dichloromethane vapour. The color can be recovered after the vapour is removed. Such fluorescence switching indicates that **2b** exhibits different states in different conditions. A similar fluorescence change of **2b** can also be observed in other solvents, such as tetrahydrofuran and chloroform. Thus, the fluorescence color changes can be used in detecting highly volatile organic solvents because they can be distinguished easily by eye.

In conclusion, we have revealed enhanced emission with large red shifts and color change of a novel benzoxazole-based derivative. In contrast to the general observation that H-aggregate formation quenches the light emission of chromophores, **2b** exhibit H-type aggregates and efficient emission in the aggregated state. The specific slip-stacking and the dimer formed by multiple intermolecular interactions avoid strong H-type coupling and are responsible for highly emissive H-type aggregates. The response to volatile organic solvents with blue/yellow fluorescent switching was also demonstrated. **2a** and **2c** show common AIEE features.

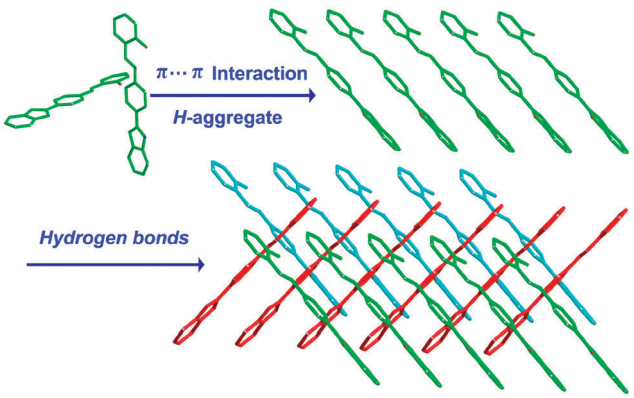

Fig. 3 Formation scheme of two-dimensional expanded cross packing layer structure of the **2b** molecules. All the hydrogen atoms are omitted for clarity.

Published on 19 May 2014. Downloaded by Washington University in St. Louis on 04/10/2014 11:10:01.

The unique enhanced emission with color changes and efficient emission is suitable for fluorescent probes and OLEDs and also provide new ideas for emissive chromophores.

We acknowledge the financial support from New Century Excellent Talents in University (China), the Doctoral Program Foundation of the Ministry of Education of China (20113401110004), the National Natural Science Foundation of China (21271003, 21271004), the Natural Science Foundation of Education Committee of Anhui Province (KJ2012A024), the Natural Science Foundation of Anhui Province (1208085MB22), the 211 Project of Anhui University, the Ministry of Education Funded Projects Focus on Returned Overseas Scholar, Higher Education Revitalization Plan Talent Project (2013) and the College Students Innovative Entrepreneurial Training Program of Anhui University (201310357025, 201310357155).

Notes and references

1 (*a*) Z. J. Zhao, J. W. Y. Lam and B. Z. Tang, *J. Mater. Chem.*, 2012, **22**, 23726–23740; (*b*) X. H. Zhu, J. B. Peng, Y. Cao and J. Roncail, *Chem. Soc. Rev.*, 2011, **40**, 3509–3524; (*c*) D. Li, H. Y. Zhang and Y. Wang, *Chem. Soc. Rev.*, 2013, **42**, 8416–8433; (*d*) Y. Zhao, L. Duan, D. Q. Zhang, G. F. Dong, J. Qiao, L. D. Wang and Y. Qiu, *ACS Appl. Mater. Interfaces*, 2014, **6**, 4570–4577.

2 (*a*) C. W. T. Leung, Y. N. Hong, S. J. Chen, E. G. Zhao, J. W. T. Lam and B. Z. Tang, *J. Am. Chem. Soc.*, 2013, **135**, 62–65; (*b*) Z. K. Wang, S. J. Chen, J. W. Y. Lam, W. Qin, R. T. K. Kwok, N. Xie, Q. L. Hu and B. Z. Tang, *J. Am. Chem. Soc.*, 2013, **135**, 8238–8245; (*c*) H. B. Shi, R. T. K. Kwok, J. Z. Liu, B. G. Xing, B. Z. Tang and B. Liu, *J. Am. Chem. Soc.*, 2012, **134**, 17972–17981; (*d*) D. Ding, K. Li and B. Z. Tang, *Acc. Chem. Res.*, 2013, **46**, 2441–2453.

3 J. D. Luo, Z. L. Xie, J. W. Y. Lam, L. Cheng, H. Y. Chen, C. F. Qin, H. S. Kwok, X. W. Zhan, Y. Q. Liu, D. B. Zhu and B. Z. Tang, *Chem. Commun.*, 2001, 1740–1741.

4 B. K. An, S. K. Kwon, S. D. Jung and S. Y. Park, *J. Am. Chem. Soc.*, 2002, **124**, 14410–14415.

5 J. B. Birks, *Photophysics of Aromatic Molecules*, Wiley, London, UK, 1970.

6 (*a*) Y. Q. Dong, J. W. Y. Lam, A. J. Qin, J. Z. Liu, Z. Li, B. Z. Tang, J. X. Sun and H. S. Kwok, *Appl. Phys. Lett.*, 2007, **91**, 011111; (*b*) C. W. T. Leung, Y. N. Hong, S. J. Chen, E. G. Zhao, J. W. Y. Lam and B. Z. Tang, *J. Am. Chem. Soc.*, 2013, **135**, 62–65; (*c*) Y. Y. Yuan, R. T. K. Kwok, G. X. Feng, J. Liang, J. L. Geng, B. Z. Tang and B. Liu, *Chem. Commun.*, 2014, **50**, 295–297.

7 (*a*) B. K. An, J. Gierschner and S. Y. Park, *Acc. Chem. Res.*, 2012, **45**, 544–554; (*b*) X. Q. Zhang, X. Y. Zhang, B. Yang, Y. L. Zhang and Y. Wei, *ACS Appl. Mater. Interfaces*, 2014, **6**, 3600–3606.

8 (*a*) X. Q. Zhang, Z. G. Chi, B. J. Xu, L. Jiang, X. Zhou, Y. Zhang, S. W. Liu and J. R. Xu, *Chem. Commun.*, 2012, **48**, 10895–10897; (*b*) M. Zheng, D. T. Zhang, M. X. Sun, Y. P. Li, S. F. Xue and W. J. Yang, *J. Mater. Chem. C*, 2014, **2**, 1913–1920; (*c*) X. Q. Zhang, Z. Y. Ma, Y. Yang, X. Y. Zhang, Z. G. Chi, S. W. Liu, J. R. Xu, X. R. Jia and Y. Wei, *Tetrahedron*, 2014, **70**, 924–929.

9 L. K. Wang, Z. Zheng, Z. P. Yu, J. Zheng, M. Fang, J. Y. Wu, Y. P. Tian and H. P. Zhou, *J. Mater. Chem. C*, 2013, **1**, 6952–6959.

10 F. S. Santos, T. M. H. Costa, V. Stefani, P. F. B. Gonalves, R. R. Descalzo, E. V. Benvenutti and F. S. Rodembusch, *J. Phys. Chem. A*, 2011, **115**, 13390–13398.

11 X. Y. Shen, Y. J. Wang, E. G. Zhao, W. Z. Yuan, Y. Liu, P. Lu, A. J. Qin, Y. G. Ma, J. Z. Sun and B. Z. Tang, *J. Phys. Chem. C*, 2013, **117**, 7334–7347.

12 (*a*) Y. Qian, M. M. Cai, X. H. Zhou, Z. Q. Gao, X. P. Wang, Y. Z. Zhao, X. H. Yan, W. Wei, L. H. Xie and W. Huang, *J. Phys. Chem. C*, 2012, **116**, 12187–12195; (*b*) X. P. Li, Y. Qian, S. Q. Wang, S. Y. Li and G. Q. Yang, *J. Phys. Chem. C*, 2009, **113**, 3862–3868.

13 Z. P. Yu, Y. Y. Duan, L. H. Cheng, Z. L. Han, Z. Zheng, H. P. Zhou, J. Y. Wu and Y. P. Tian, *J. Mater. Chem.*, 2012, **22**, 16927–16932.

14 Y. N. Hong, J. W. Y. Lam and B. Z. Tang, *Chem. Soc. Rev.*, 2011, **40**, 5361–5388.

15 (*a*) D. Oelkrug, A. Tompert, J. Gierschner, H. J. Egelhaaf, M. Hanack, M. Hohloch and E. Steinhuber, *J. Phys. Chem. B*, 1998, **102**, 1902–1907; (*b*) K. H. Schweikart, M. Hohloch, E. Steinhuber, M. Hanack, L. Lüer, J. Gierschner, H. J. Egelhaaf and D. Oelkrug, *Synth. Met.*, 2001, **121**, 1641–1642; (*c*) J. Gierschner, L. Lüer, B. Milián-Medina, D. Oelkrug and H. J. Egelhaaf, *J. Phys. Chem. Lett.*, 2013, **4**, 2686–2697.

 This journal is © The Royal Society of Chemistry 2014